

Optical, structural, FTIR and photoluminescence characterization of Cu and Al doped CdS thin films by chemical bath deposition method

S. Hemathangam¹ · G. Thanapathy² · S. Muthukumar³

Received: 29 January 2016 / Accepted: 1 March 2016 / Published online: 8 March 2016
© Springer Science+Business Media New York 2016

Abstract Pure CdS, Cd_{0.96}Cu_{0.04}S and Cd_{0.94}Cu_{0.04}Al_{0.02}S thin films have been synthesized by simple chemical deposition method. Cubic structure noticed in undoped CdS and Cu-doped CdS thin films was changed into mixer of cubic and hexagonal structure for Cd_{0.94}Cu_{0.04}Al_{0.02}S. The change in crystallite size, peak position and lattice parameters were discussed based on thickness, crystal structure and the density of defect states. Microstructure of the synthesized films was investigated by scanning electron microscope and energy dispersive X-ray spectra which confirmed the presence of compositional elements such as Cd, S, Cu and Al. Higher thickness and the enhanced crystallite size were responsible for the higher absorption in Cd_{0.96}Cu_{0.04}S than other films. The higher energy gap (2.56 eV) and enhancement of visible light absorption noticed in Cd_{0.96}Cu_{0.04}S thin film led them as an effective way to utilize solar energy and enhance its photocatalytic activity under visible light. The accelerated I_G/I_{UV} ratio noticed in Al, Cu co-doped CdS film was due to the formation of new energy levels related to defect states produced by Al/Cu impurities and mixer of hexagonal and cubic structure

1 Introduction

Optical, electronic and structural properties of semiconducting nanocrystals have gained prominence due to their great potential in many applications ranging from DNA makers to light emitting displays (LEDs) owing to their unique size dependent optical and electronic properties [1, 2]. Specifically, sulfide based phosphors such as ZnS and CdS (E_g ~ 3.7 and ~2.5 eV, respectively) [3–5] have been potential candidates for their promising applications in electro-luminescent (EL), photoluminescent (PL) and photoconductive (PC) devices.

Li et al. [6], studied the room temperature PL spectra of ZnO thin films with a strong near band-edge emission at 380 nm and a negligible deep-level emission around 530 nm, indicating the concentrations of the defects responsible for deep-level emissions are reduced on annealing. Zhay et al. [7] characterized the optical properties of Cu₂O films by the ultraviolet–visible (UV–Vis) spectrum, which demonstrated the band gap changing from 2.21 to 2.43 eV with different electrochemical deposition time owing to the quantum confinement effect. Cu₂O quantum dots (QDs) decorated ZnO nanorod arrays (ZNAs) were fabricated by Zou et al. [8] using a facile hydrothermal method followed by a chemical bath deposition (CBD) process. For improving the photovoltaic stability, a protective layer was prepared on the Cu₂O QDs by a simple process of heat treatment in ambient air at 100 °C for 2 h. The results demonstrate that the passive CuO layer could be an effective protective layer to increase the photovoltaic stability. Fang et al. [9] demonstrated the fabrication of dye-sensitized solar cells (DSSCs) based on different ZnO nanostructures with controllable morphologies synthesized via capping agent-assisted hydrothermal method. DSSCs showed significantly improved photovoltaic performance

✉ S. Muthukumar
drsmk123@yahoo.co.in

¹ Department of Physics, Dharmapuram Adhinam Arts College, Dharmapuram, Mayiladuthurai 609001, Tamilnadu, India

² Department of Physics, Poompuhar College, Melaiyur, Nagapattinam District 609107, Tamilnadu, India

³ PG and Research Department of Physics, Government Arts College, Melur, Madurai 625106, Tamilnadu, India

with open-circuit voltage increasing from 0.45 to 0.73 V. Nitrogen self-doped graphitic carbon nitride (C_3N_{4+x}) was successfully synthesized by the co-thermal condensation of the precursor with a nitrogen-rich additive [10]. The average hydrogen evolution rate for C_3N_{4+x} was 1.8 times higher than that of pristine graphitic carbon nitride, and the superiority lay in greatly improved optical, emission and electronic properties of the nitrogen modified carbon nitride.

It is well known that Cu doping may provide two defect charge states viz. Cu^+ and Cu^{2+} [11]. The substitution of Cu^+/Cu^{2+} for Cd^{2+} behaves as an acceptor. The ionic radii of Cd^{2+} and Cu^+/Cu^{2+} are 0.97 Å and 0.77/0.73 Å, respectively. So, Cu can easily be substituted in the place of Cd either in substitutional or interstitial positions [12]. Therefore, Cu is selected as one of the doping elements with CdS. Conductivity of CdS thin films is increased by Al doping. During Al doping in CdS, Al^{3+} ions are properly entered into Cd site at lower concentration and interstitially at high concentration and the interstitial ions will act as recombination centers [13]. Therefore, Al is selected as second doping element with Cu-doped CdS.

CdS and transition metal TM-doped CdS have been prepared using various techniques, such as thermal evaporation [14], electro-deposition [15], chemical bath deposition [16], and spray pyrolysis [17]. Among the different techniques, a well established chemical deposition technique [18] is used to prepare the TM-doped and TM co-doped CdS thin films because it is one of the low cost and more suitable methods for large area deposition.

The control the morphology, particle size and optical properties of the film are possible by controlling the level of Cu and Al doping during synthesis. Even though some works have been already carried out on Cu-doped CdS [11, 12] or Al-doped CdS system [13, 18], the comparative studies of optical, structural and photoluminescence behaviour of Cu, Al co-doped CdS is still scanty. Therefore, in the present investigation the structural, optical and morphological properties of Cu-doped CdS and Cu, Al co-doped CdS thin films have been investigated systematically. The chemical bonding present in the samples was investigated by FTIR spectra to get a better understanding of the deterioration characteristics of the samples. Finally, photoluminescence properties in addition to XRD study were discussed to investigate the microstructural properties of the samples.

2 Experimental

2.1 Substrate cleaning

Substrate cleaning is very important in the deposition of thin films. The un-cleaned substrate results the non-

uniform film growth. In order to avoid the non-uniform film growth, the glass slides of dimensions $26 \times 76 \times 2 \text{ mm}^3$ were boiled in chromic acid for 2 h and kept in it for 12 h. Then, they were washed with detergent, and again rinsed in acetone before the deposition of the films. The cleaned substrate was kept dipped in de-ionized water before use.

2.2 Preparation of CdS, $Cd_{0.96}Cu_{0.04}S$ and $Cd_{0.94}Cu_{0.04}Al_{0.02}S$ thin films

For the preparation of Cu doped CdS thin films, cadmium chloride monohydrate ($CdCl_2 \cdot H_2O$), copper chloride dihydrate ($CuCl_2 \cdot 2H_2O$), aqueous ammonia solution, Thiourea ($(NH_2)_2CS$), ammonium chloride (NH_4Cl) were used without further purification. All the chemicals used in the present investigation were analytical grade with more than 99 % purity purchased from Merc. The precursors $CdCl_2 \cdot H_2O$, $CuCl_2 \cdot 2H_2O$ and $CS(NH_2)_2$ were used as source materials of Cd^{2+} , Cu^{2+} and S^{2-} ions respectively.

The deposition bath was prepared by the addition of appropriate amount of 0.996 M $CdCl_2$, 2.5 M NH_4Cl and double distilled water in 100 ml beaker. The solution was stirred well with the help of magnetic stirrer to make a homogeneous solution. Al doping was carried out by adding the appropriate amount of 0.004 M $CuCl_2 \cdot 2H_2O$ to the main solution. The 40 ml 1 M $(NH_2)_2CS$ solution was prepared separately and added slowly into the deposition bath. The pH of the solution was maintained as 10 using aqueous ammonia solution. The solution was stirred well with the help of magnetic stirrer for a few seconds and then well cleaned glass substrates were slowly introduced into the bath vertically. The temperature of the mixed solution was maintained at 80 °C (353 K) during the whole reaction process. The reactants were vigorously stirred under air atmosphere. The films deposited on glass substrates have been taken out after 2 h and cleaned several times with de ionized water and alcohol to remove loosely bounded ions/atom. Cleaning of the film is very important to remove the surface impurities and minimize the particle agglomeration. After the deposition, films were dried using micro-oven at 50–80 °C for 30 min. The prepared films by this method were uniform and well adherent to the substrate. Transparent and homogenous yellowish coloured thin films were obtained at the end of deposition process.

For the preparation of Cu, Al co-doped CdS thin films both copper chloride dihydrate ($CuCl_2 \cdot 2H_2O$), and Aluminium sulphate ($Al_2(SO_4)_3 \cdot 16H_2O$) were used as a source materials. Yellow colour of CdS film was changed into yellowish orange when Cu = 4 % is doped into CdS which is changed into dark yellowish orange for additional 2 % of Al doping as shown in Fig. 1. In the present investigation Tolansky's method was employed to find the thickness

(t) of the thin films. The accuracy of the thickness measurement is ± 3 nm [19].

2.3 Characterization techniques

The crystal structure of the synthesised thin films was determined by powder X-ray diffraction (XRD). XRD patterns are recorded on a RigakuC/max-2500 diffractometer using $\text{CuK}\alpha$ radiation ($\lambda = 1.5406 \text{ \AA}$) at 40 kV and 30 mA from $2\theta = 10^\circ$ to 80° . Scanning electron microscope (SEM) technique is used to observe the particle sizes, rough morphology and distribution of the particles on the surface of the system. The surface morphology of the prepared films was studied using a scanning electron microscope (SEM, Philip XL 30). The topological features and the composition of Cd, Cu, Al and S were determined by energy dispersive X-ray spectrometer (EDX) on K and L lines.

The UV–visible optical absorption and transmittance spectra are carried out with a view to explore their optical properties. The spectral absorption of the films is determined using UV–visible spectrometer (Model: Lambda 35, Make: Perkin Elmer) in the wavelength range from 300 to 900 nm using cm^{-1} quartz cuvettes at room temperature. Halogen and deuterium lamps are used as sources for visible and UV radiations, respectively at room temperature. The presence of chemical bonding was studied by FTIR spectrometer (Model: Perkin Elmer, Make: Spectrum RX I) in the range of $400\text{--}4000 \text{ cm}^{-1}$. A bare glass substrate is used for base line correction of the system before recording the FTIR spectra of the samples. The photoluminescence (PL) spectra of the thin films have been carried out between the wavelength ranging from 340 to 580 nm using a fluorescence spectrophotometer (Model: F-2500,

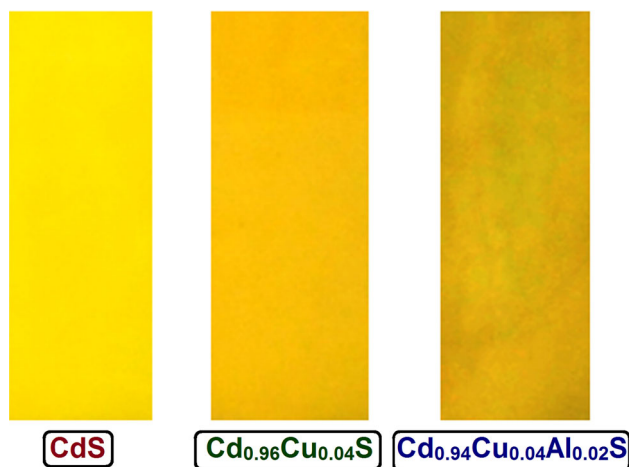


Fig. 1 Variation of colour change for different thin films such as CdS (yellow), Cu-doped CdS (yellowish orange) and Al, Cu co-doped CdS (dark yellowish orange) (Color figure online)

Make: Hitachi) at room temperature. A Xenon lamp with a wavelength of 330 nm and power of 150 W is used as the excitation source.

3 Results and discussion

3.1 Structural characteristics

The typical XRD patterns of CdS, Cu-doped CdS and Cu, Al co-doped CdS thin films between 10° and 80° are as shown in Fig. 2. The broad hump in the 2θ range of $15^\circ\text{--}35^\circ$ is mainly due to the amorphous glass substrate. The similar result was observed by Nair et al. [20] in Cu_xS thin films. As shown in Fig. 2, undoped CdS thin film exhibits three major diffraction peaks corresponding to the (111), (220) and (311) with a preferred orientation along (111) plane. The phase purity of the sample was confirmed by XRD diffraction peaks i.e., no extra peaks for oxides/sulphides of CdS or other phases are found. The data are fitted with $\text{CuK}\alpha$ profile to find the peaks corresponding to CdS thin films. The corrected spectra matched with the JCPDS card No. 89-0440 corresponding to cubic phase.

Based on different conditions, CdS nanocrystals exhibit four different forms such as cubic (zinc blende), hexagonal

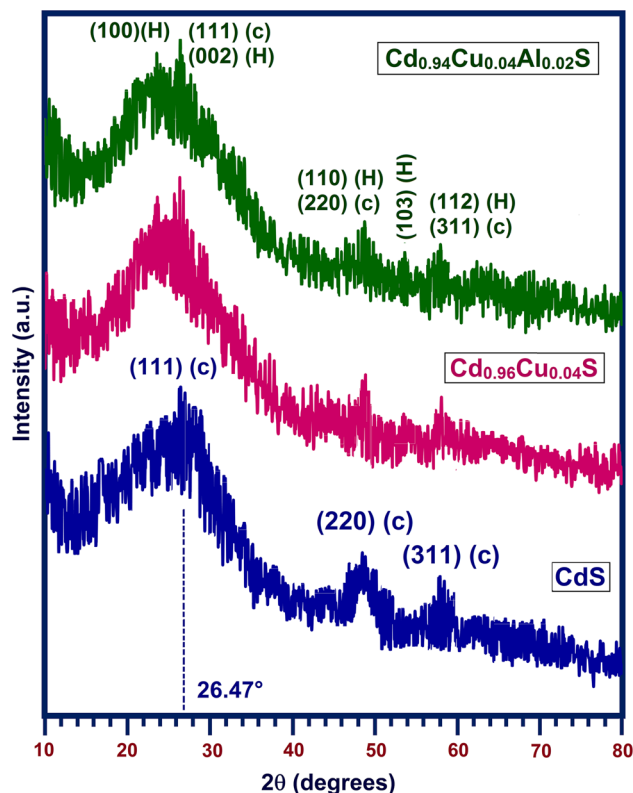


Fig. 2 X-ray diffraction pattern of pure CdS, Cu-doped CdS and Al, Cu co-doped CdS thin films at room temperature

(wurtzite), distorted rock salt, and cubic rock salt [21]. At room temperature, cubic CdS is considered a metastable phase while hexagonal CdS is the stable phase and thermal annealing may cause a phase transition from the cubic phase to the hexagonal phase. According to the heterogeneous reaction, it is argued that the ion by ion process results the uniform films with pure hexagonal or cubic phase or mixed hexagonal phase [22]. In the present case, reaction occurs at room temperature and hence crystallographic phase of CdS film grown by heterogeneous process is cubic. A lot of results on CdS samples growth by chemical synthesis support the fact that CdS nanoparticles grow in cubic phase in the 70–80 °C range [23, 24].

Meanwhile, the (111) plane shows a considerable increase in intensity upon incorporation of Cu. The similar increase in intensity of doped CdS was observed by Afify et al. [25] which could be attributed to the change in the scattering factor corresponding to the incorporated element, or the decrease in the crystallite size, or both. The dominant (111) plane is shifted to higher angle side by Cu-doping which is a consequence of the incorporation of Cu into CdS [26]. When Al is co-doped with Cd–Cu–S, the cubic phase turned to the mixed phase of cubic and hexagonal. This mixed phase is prominently exposed by the additional diffraction peaks at 2θ values of 24.7° (1 0 0), 26.5° (0 0 2), 43.7° (1 1 0), 47.8° (1 0 3), 51.9° (1 1 2) were observed. Substitution of more co-ordination numbered (12) Al^{3+} into the position of less co-ordination numbered (8) Cd^{2+} increases the number of surrounding atom and hence an additional hexagonal phase is introduced in the cubic phased CdS thin film by Al doping. So, CdS and Cu-doped CdS existed only in cubic phase, but Al–CdS existed mixed crystals of cubic and hexagonal phases. The decrease in intensity of (111) plane and its peak position shift towards lower angle side compared with Cu-doped CdS are due to the incorporation of Al^{3+} ions which acts as both proper substitution and interstitial position.

The variation of peak position (2θ), full width at half maximum (FWHM), d-value, cell parameter, average crystallite size (D), and microstrain (ϵ) along (111) plane of CdS, $\text{Cd}_{0.96}\text{Cu}_{0.04}\text{S}$ and $\text{Cd}_{0.94}\text{Cu}_{0.04}\text{Al}_{0.02}\text{S}$ thin films are given in Table 1. The film thickness of pure CdS is found to be 0.88 μm . During the substitution of Cu, the film thickness is increased to 1.03 μm . The observed higher thickness for Cu-doped CdS is due to the higher growth rate of the film. The released high amount of Cd^{2+} , Cu^{2+} and S^{2-} ions from bound state during reaction deposited on the surface of the glass substrate which enhance the growth rate and hence the thickness of the film. The further doping of Al into Cu-doped CdS reduces the film thickness to 0.92 μm . The available number of Al^{3+} ions from its

source $\text{Al}_2(\text{SO}_4)_3$ is low than Cd^{2+} ions and Cu^{2+} ions. This slow released rate of Al^{3+} ions is responsible for the reduction of film thickness.

The interplanar distance ($d = 3.365 \text{ \AA}$) and the cell parameter ($a = 5.829 \text{ \AA}$) of CdS thin films are reduced to $d = 3.344 \text{ \AA}$ and $a = 5.791 \text{ \AA}$ when Cu is introduced into Cd-S lattice. It has been reported that Cu^+ and Cu^{2+} are the ionic states found in Cd^{2+} sites into the CdS lattice [27]. If Cu^+ (ionic radius = 0.74 \AA) and Cu^{2+} (ionic radius = 0.71 \AA) enter substitutionally in Cd^{2+} (ionic radius = 0.94 \AA) sites, the lattice will tend to reduce the volume. This decrease in d-value is due the substitution of $\text{Cu}^{2+}/\text{Cu}^+$ ions which have lower ionic radius in place of Cd^{2+} ions which have higher ionic radius. The interplanar distance $d_{(111)}$ is calculated using the formula $\lambda = 2d \sin \theta$. The presence of Cu in the CdS volume introduces internal stress, which distorts the crystalline lattice and provokes disorder. Internal stress is that which does not come from external forces to the volume of material as that produced by substrate mismatch or by hydrostatic pressure [23]. The distortion affects the inter-atomic distance ‘a’, similarly as has been reported for Cu-doped CdSe nanocrystals [28]. The S vacancies generation and the occupation of Cd^{2+} sites by Cu^+ and Cu^{2+} ions could be some of the reasons for the shrinkage of the CdS lattice and the tendency of amorphization when Cu enters in substitutional positions. When Al^{3+} ions are introduced into Cu-doped CdS, the values of ‘d’ and ‘a’ are slightly increased. Even though the ionic radius of Al^{3+} ions (0.5 \AA) is smaller than Cu and Cd ions [29], ‘d’ value and lattice parameter ‘a’ are increased by Al-doping which is due to the formation of defect states and distortion.

The average crystal size of the film is calculated from the diffraction peaks along (111) plane using Debye–Scherrer’s formula [30]:

$$\text{Average crystallite size (D)} = \frac{0.9\lambda}{\beta \cos \theta} \quad (1)$$

where, ‘ λ ’ is the wave length of X-ray used (1.5406 \AA), ‘ β ’ is the angular peak width at half maximum in radian along (111) plane, and ‘ θ ’ is the Bragg’s diffraction angle. The micro-strain (ϵ) can be calculated using the formula [31]:

$$\text{Micro-strain } (\epsilon) = \frac{\beta \cos \theta}{4} \quad (2)$$

Full widths at half maximum (β) along (111) plane of the XRD peaks for Cu-doped CdS (3.24°) is smaller than CdS (2.91°). This result shows that the grain growth of CdS was promoted by Cu incorporation which increases the average crystallite size from 2.52 nm (CdS) to 2.81 nm. The similar enhanced crystallite size by Cu-doping was noticed in the literature [26, 32]. The reduction in strain from 7.95×10^{-3} (CdS) 7.13×10^{-3} (Cu-doped CdS) is

Table 1 The variation of Peak position (2 θ), full width at half maximum (FWHM), d-value, cell parameter, average crystallite size (D), and microstrain (ϵ) along (111) plane of CdS, Cd_{0.96}Cu_{0.04}S and Cd_{0.94}Cu_{0.04}Al_{0.02}S thin films

Samples	Thickness (t) (μm)	Peak position (2 θ) (degrees)	FWHM (degrees)	d _z -value (\AA)	Cell parameter a = b = c (\AA)	Average crystallite size (D) (nm)	Micro strain (10^{-3})
CdS	0.88	26.47	3.24	3.365	5.829	2.52	7.95
Cd _{0.96} Cu _{0.04} S	1.03	26.62	2.91	3.344	5.791	2.81	7.13
Cd _{0.94} Cu _{0.04} Al _{0.02} S	0.92	26.51	3.07	3.359	5.818	2.66	7.53

another possible for the better crystallization. FWHM value is increased to 3.07° when Al is substituted into Cu-doped CdS. The increased FWHM is correlated with the decrease of crystallite size to 2.66 nm. The induced higher strain (7.53×10^{-3}) by Al-doping is another factor for the deterioration crystallite size.

3.2 Morphology and compositional studies

The typical EDX spectra of pure CdS, Cd_{0.96}Cu_{0.04}S and Cd_{0.94}Cu_{0.04}Al_{0.02}S thin films are shown in Fig. 3a–c, respectively. The inset of Fig. 3 shows the surface morphology carried out by SEM. The quantitative atomic percentage of the compositional elements present in undoped CdS, Cd_{0.96}Cu_{0.04}S and Cd_{0.94}Cu_{0.04}Al_{0.02}S thin films using EDX analysis are presented in Table 2.

The atomic percentage of Cd and S are found to be 56.87 and 43.13 for pure CdS thin film which shows Cd rich phase. The surface morphology of CdS film (Fig. 3a) reveals the un-even distribution of grains in the cluster form throughout the surface with a compact and fine grained morphology. Shape of the grains in this sample is a mixture of spherical-like and rod-like nature. When Cu is added into CdS, the surface morphology turned into uniform distribution of grains throughout the sample with spherical shape as shown in Fig. 3b. Moreover, the average grain size of Cd_{0.96}Cu_{0.04}S film is enhanced as noticed in Table 1.

The existence of lower micro-strain and the reduction of lattice imperfection and defects in Cd_{0.96}Cu_{0.04}S are responsible for the improvement of crystallite size. The EDX spectra of Cd_{0.96}Cu_{0.04}S thin film shows the well defined peaks corresponding to Cd, S and Cu (Fig. 3b). The cluster formations surrounded by the pores was observed in the Cd_{0.94}Cu_{0.04}Al_{0.02}S thin film as shown in Fig. 3c. The presence of more defects and deformed lattice structure by Al³⁺ ions in Cd–Cu–S causes the uneven surface morphology. The EDX analysis confirms their nominal percentage and chemical purity of system. It is observed from Fig. 3b that Cu/(Cd + Cu) ratio is derived to be 4.27 %. Similarly, Cu/(Cd + Cu + Al) and Al/(Cd + Cu + Al) ratio are derived to be 3.98 and 1.85 % for

Cd_{0.94}Cu_{0.04}Al_{0.02}S thin films (Fig. 3c). The atomic percentage of Cu in Cd_{0.96}Cu_{0.04}S thin film and the percentage of Al in Cd_{0.94}Cu_{0.04}Al_{0.02}S thin film are very close to their nominal stoichiometry within the experimental error.

3.3 Optical study

The optical properties including transmission, refractive index and energy gap are of great importance for the study of window layer material in solar cell. The optical absorption spectra of pure CdS, Cd_{0.96}Cu_{0.04}S and Cd_{0.94}Cu_{0.04}Al_{0.02}S thin films are recorded at room temperature ranging from 300 to 900 nm as shown in Fig. 4. Since the variation of optical absorption is not clear for pure CdS, the clear and high resolution absorption spectra of CdS thin film is given as inset of Fig. 4. Doping of Cu in CdS enhances the optical absorption and also shifts the optical absorption edge towards lower wavelength side; this shift represents the enhancement in optical band gap. Even though the absorption edge shifts towards lower wavelength side, the absorption peak of Cu-doped CdS moves towards the higher wavelength side. Cu-doping reduces the defects in CdS thin film and reorients the sample into better crystallization. The structural deformation generated by Cu-doping leads to absorption of incident photons and a substitutional dissolution which yield an improvement in grain structure of the film [33]. The higher thickness and hence the enhanced crystallite size are also responsible for the higher absorption. The distortion produced by Al³⁺ ions and the formation of defect states and secondary phases which were not detected by XRD measurements due to its limitation reduce the absorption intensity of Al-doped Cd_{0.96}Cu_{0.04}S thin film.

The typical room temperature transmittance spectra of pure CdS, Cd_{0.96}Cu_{0.04}S and Cd_{0.94}Cu_{0.04}Al_{0.02}S thin films in the wavelength between 300 and 900 nm are shown in Fig. 5. The inset of Fig. 5 shows the high resolution transmittance spectra of CdS thin film to get the better insight of the film. The transmittance spectrum reflects just opposite trend of absorption spectrum and shows the poor transmittance nature of doped films than CdS. All the films exhibit low transmittance in UV region and high transmittance in the visible region. The reduced transmittance at

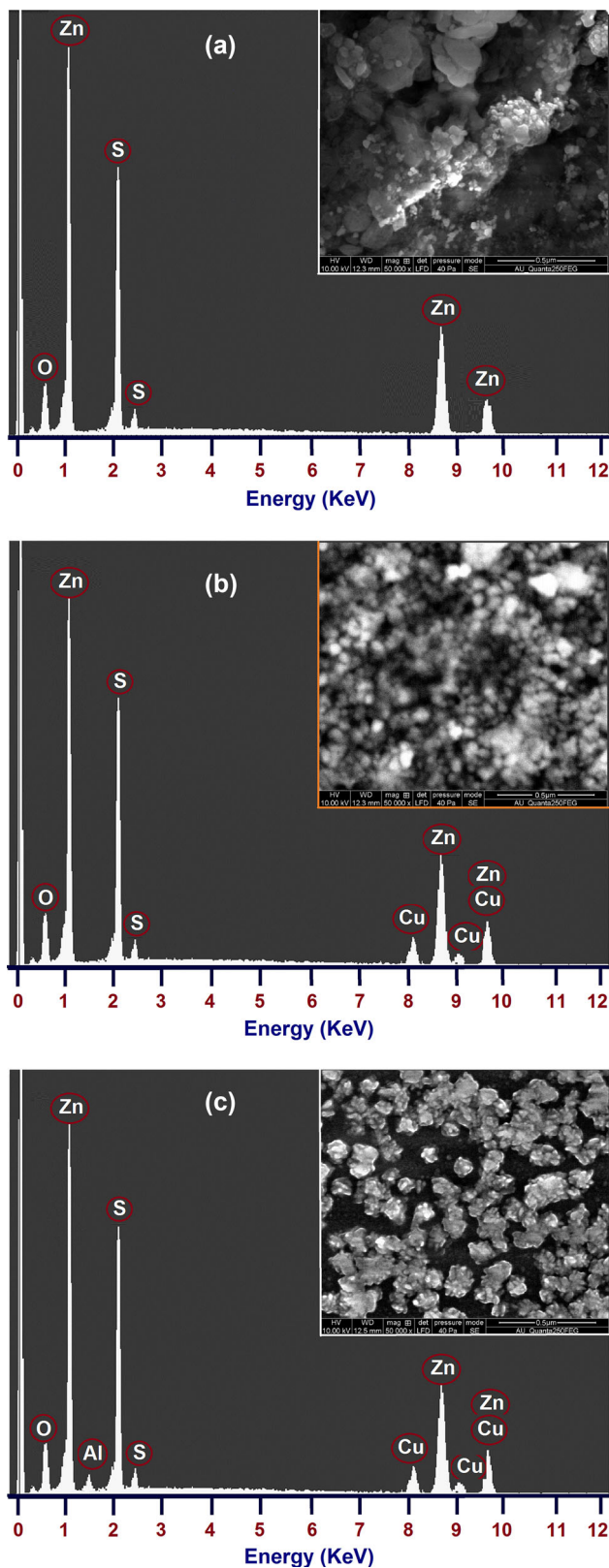


Fig. 3 Energy dispersive X-ray (EDX) spectra of **a** undoped CdS thin film, **b** Cd_{0.96}Cu_{0.04}S thin film and **c** Cd_{0.94}Cu_{0.04}Al_{0.02}S thin film at room temperature. The *inset* shows their scanning electron microscope images

Cu-doped CdS film is due to the improved crystallization. This is because the transmittance of the films decreases with grain size in the visible region of spectrum due to light scattering on their rough surfaces [34]. The higher growth rate i.e., better thickness and packing density noticed is another reason for the observed low transmittance [35] in Cu-doped CdS thin film because both thickness and packing density have inverse relationship with transmittance. Al-doping into Cd–Cu–S improves the transmittance than Cu-doped CdS. This higher transmittance can be attributed to more voids and so the lower packing density of the film. Another observation about these transmission spectra is that the absorption edge shifts towards higher wavelength side. The noticed changes in the absorption and transmittance transmission are due to the thickness variation and the fundamental differences in the film absorption [36].

The energy gap varies with the change in several parameters like grain size, structural parameters, carrier concentration and lattice strain. The film thickness has direct dependence on the lattice parameters, grain size and strain. The energy gap of CdS samples changes with respect to thickness due to lattice strain [37]. The optical band gap of Cu-doped and Al, Cu co-doped CdS thin films can be calculated by using the Tauc’s equation which demonstrates a relationship between absorption coefficient and the incident photon energy of semiconductors. The optical band gap is evaluated using the Tauc relation [38]:

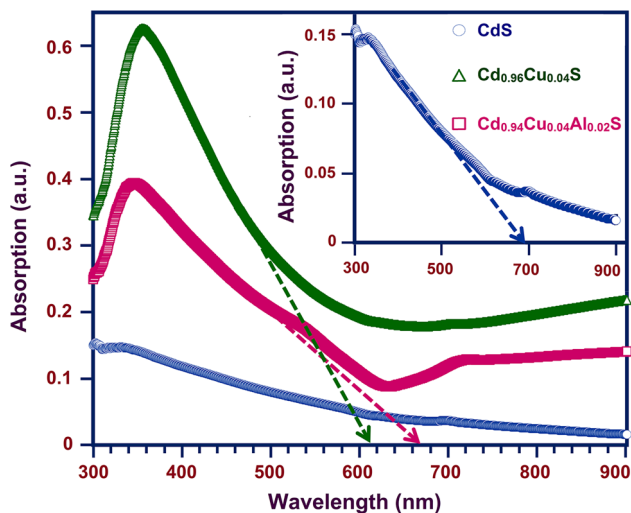
$$ah\nu = A(h\nu - E_g)^n \tag{3}$$

where, A as a constant, E_g is optical band gap of the material and the exponent n depends upon the type of transition. In our case, n is taken as 1/2. The energy band gap (E_g) of the synthesized thin films can be obtained by plotting (αhν)² versus hν and extrapolating the linear portion of the absorption edge as shown in Fig. 6.

The energy band gap (E_g) of as deposited CdS, Cd_{0.96}Cu_{0.04}S and Cd_{0.94}Cu_{0.04}Al_{0.02}S thin films can be estimated by plotting (αhν)² versus hν as shown in Fig. 6. The inset of Fig. 6 shows the clear plot of (αhν)² versus hν for CdS thin film. The energy gap of as-deposited CdS thin film is found to be 2.42 eV [39]. In the present case it is calculated as 2.40 eV. The substitution of Cu improves the band gap from 2.40 eV (CdS) to 2.56 eV (ΔE_g ≈ 1.6 eV). The higher energy gap (2.56 eV) and enhancement of visible light absorption noticed in Cd_{0.96}Cu_{0.04}S thin film has been though as an effective way to utilize solar energy and enhance its photocatalytic activity under visible light. At the same time the energy gap is reduced to 2.49 eV (red shift) for Al, Cu co-doped thin film. The incorporation of Al³⁺ induces the sulfur deficiency in Cd–Cu–S lattice as supported by EDX spectra (Table 2). The similar sulfur

Table 2 The quantitative atomic percentage of the compositional elements present in of pure CdS, Cd_{0.96}Cu_{0.04}S and Cd_{0.94}Cu_{0.04}Al_{0.02}S thin films using EDX analysis

Samples	Atomic percentage of the elements (%)				Cu/(Cd + Cu + Al) (%)	Al/(Cd + Cu + Al) (%)
	Cd	S	Cu	Al		
CdS	56.87	43.13	–	–	–	–
Cd _{0.96} Cu _{0.04} S	55.26	42.38	2.36	–	4.27	–
Cd _{0.94} Cu _{0.04} Al _{0.02} S	54.93	41.67	2.32	1.08	3.98	1.85

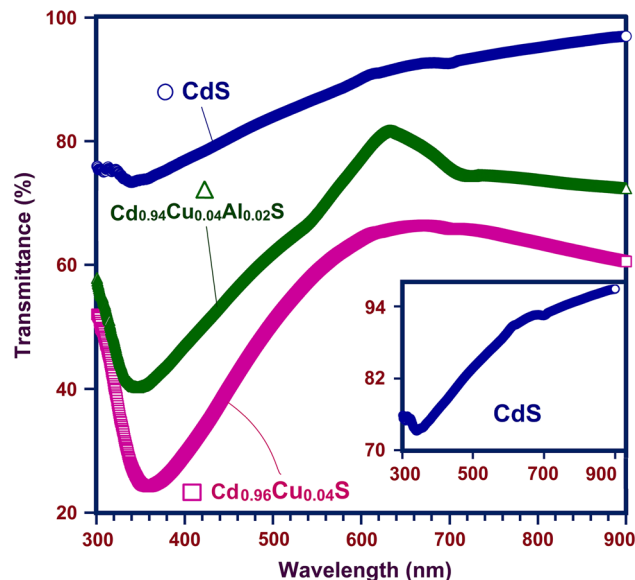
**Fig. 4** UV–visible absorption spectra of undoped CdS, Cu-doped CdS and Al, Cu co-doped CdS thin films as a function of wavelength from 300 to 900 nm at room temperature. The inset shows the magnified absorption spectra for CdS thin film

deficiency was reported in Al-doped CdS [40]. The sulfur deficiency increases the donor levels in the band gap of CdS. Under this condition donor levels become degenerate and merge in the conduction band of CdS, causing the conduction band to extend into the band gap which reduces the band gap.

3.4 Photoluminescence (PL) spectra

II–VI semiconductors have high intrinsic photoluminescence (PL) quantum efficiency due to direct band transitions [41]. PL spectrum is used to correlate the structure and optical property of CdS and TM-doped CdS thin films which originate from recombination of surface states [42]. The room temperature PL spectra of the synthesized thin films in the wavelength range from 340 to 580 nm are shown in Fig. 7a.

PL spectra of CdS film consists of a strong UV band centered at 360 nm, a weak blue band centered at 494 nm and broad and weak green band around 540 nm. UV

**Fig. 5** Transmittance spectra of undoped CdS, Cu-doped CdS and Al, Cu co-doped CdS thin films as a function of wavelength from 300 to 900 nm at room temperature. The inset shows the magnified absorption spectra for CdS thin film

emission band is commonly originates from excitonic recombination corresponding to the near-band-edge (NBE) emission. Generally, the wavelength corresponding to UV emission represents the energy gap of the material. When Cu is substituted into CdS, it acted as optically active luminescence centers and efficiently created the luminescence of particle. After Cu-doped step, the luminescent centers were transferred to impurity ions. During Cu-doping, both UV emission and defect related blue and green band emissions are enhanced. The increase of UV intensity by Cu-doping represents the improvement in optical quality of the film as evidenced by XRD studies.

Moreover, the emission peaks after 470 nm contain broad and splits into multiple peaks. Defect related visible emissions may be ascribed to the intrinsic defects such as oxygen vacancies (Vo), oxygen interstitials (Oi), Cu/Al interstitials and oxygen antisites (O_{Zn}) [43]. A weak blue band around 494 nm along with their shoulders at 506 and

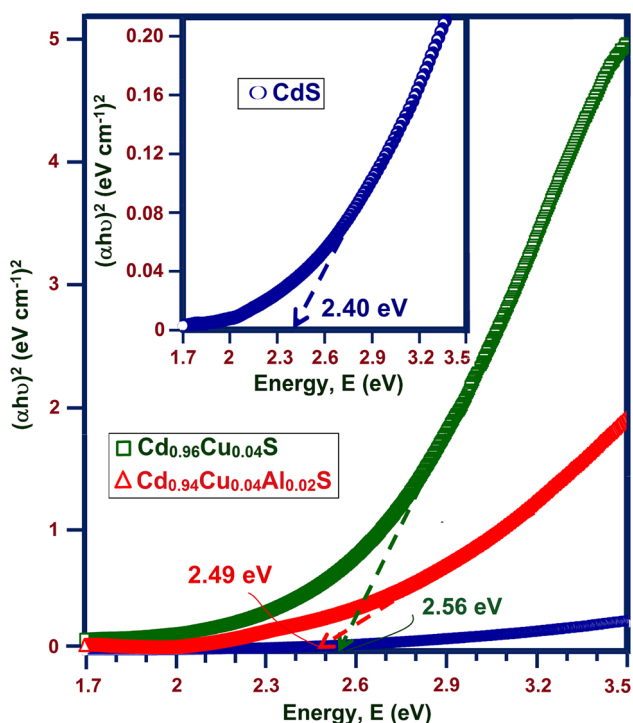


Fig. 6 The $(\alpha h\nu)^2$ versus $h\nu$ curves for the optical band gap determination of undoped CdS, Cu-doped CdS and Al, Cu co-doped CdS thin films. The inset shows the magnified image for CdS thin film

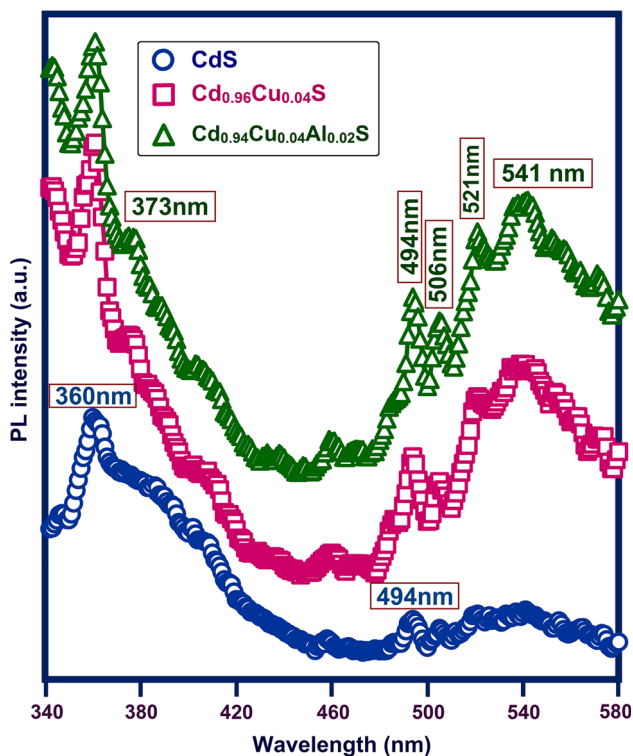


Fig. 7 Room-temperature photoluminescence spectra of undoped CdS, Cu-doped CdS and Al, Cu co-doped CdS thin films using 330 nm line of Xe excitation source

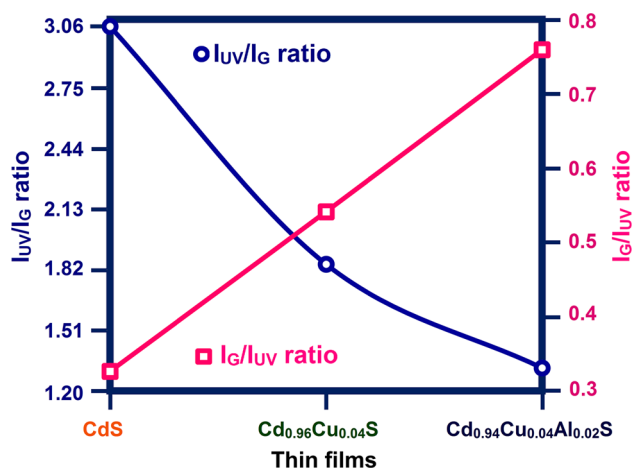


Fig. 8 The variation of I_{UV}/I_G ratio and I_G/I_{UV} ratio for CdS, Cu-doped CdS and Al, Cu co-doped CdS thin films

521 nm are observed in Cu-doped CdS. The blue band emission is originated from the interstitial position of Cd^{2+} ions. It is explained by the transition from extended Cd_i states, which are slightly below the Cd_i band and valence band. The excited electrons relax to extended Cd_i states and transit to the valence band with the emission of blue light. In addition, a broad green band emission centered at 541 nm is observed in Cu-doped CdS. The origin of green band emission is due to radiative recombination of electrons and holes via the surface/defect states present [44].

Figure 7b shows the variation of intensity of UV (I_{UV}) band and green band ratio for CdS, $Cd_{0.96}Cu_{0.04}S$ and $Cd_{0.94}Cu_{0.04}Al_{0.02}S$ thin films. The recombination of electrons trapped inside a sulfur vacancy with a hole in the valence band of the CdS is responsible for green band emission for CdS. The accelerated I_G/I_{UV} ratio noticed in Al, Cu co-doped CdS film is due to the formation of new energy levels related to defect states produced by Al/Cu impurities and mixer of hexagonal and cubic structure. The defects states induce more electronic transitions which lead to greater PL intensity. The tuning of visible emissions (both blue and green bands) by Cu/Al doping have a great potential in the nano-scaled optoelectronic devices (Fig. 8).

4 Conclusion

Following are the conclusions drawn from the present studies:

- Pure CdS, Cu $Cd_{0.96}Cu_{0.04}S$ and $Cd_{0.94}Cu_{0.04}Al_{0.02}S$ thin films have been synthesized by simple chemical deposition method.
- Cubic structure noticed in undoped CdS and Cu-doped CdS thin films is changed into mixer of cubic and hexagonal structure for Al, Cu co-doped CdS.

- The change in crystallite size, peak position and lattice parameters are discussed based on thickness, crystal structure and defect states induced by impurity.
- Microstructure of the synthesized films is investigated by SEM. EDX spectra confirmed the presence of compositional elements such as Cd, S, Cu and Al.
- Higher thickness and the enhanced crystallite size are responsible for the higher absorption in Cd_{0.96}Cu_{0.04}S than other films.
- The higher energy gap (2.56 eV) and enhancement of visible light absorption noticed in Cd_{0.96}Cu_{0.04}S thin film reveal that the present film is used for effective utilization of solar energy and enhance its photocatalytic activity under visible light.
- The accelerated I_G/I_{UV} ratio noticed in Al, Cu co-doped CdS film is due to the formation of new energy levels related to defect states produced by Al/Cu impurities and mixer of hexagonal and cubic structure.

References

1. T. Song, F. Zhang, X. Shen, X. Zhang, X. Zhu, B. Sun, *Appl. Phys. Lett.* **95**, 233502 (2009)
2. D. Shao, A. Xia, J. Hu, C. Wang, W. Yu, *Colloids Surf. A* **322**, 61 (2008)
3. A. Datta, S.K. Panda, S. Chaudhuri, *J. Phys. Chem. C* **111**, 17260 (2007)
4. Y.P.V. Subbaiah, P. Prathap, K.T. Ramakrishna Reddy, *Appl. Surf. Sci.* **253**, 2409 (2006)
5. L. Wang, H. Wei, Y. Fan, X. Liu, J. Zhan, *Nanoscale Res. Lett.* **4**, 558 (2009)
6. J. Li, H. Fan, X. Jia, J. Chen, Z. Cao, X. Chen, *J. Alloys Compd.* **481**, 735 (2009)
7. Y. Zhaiy, H. Fan, Q. Li, W. Yan, *Appl. Surf. Sci.* **258**, 3232 (2012)
8. X. Zou, H. Fan, Y. Tian, M. Zhang, X. Yan, *RSC Adv.* **5**, 23401 (2015)
9. J. Fang, H. Fan, H. Tian, G. Dong, *Mater. Charact.* **108**, 51 (2015)
10. J. Fang, H. Fan, M. Li, C. Long, *J. Mater. Chem. A* **3**, 13819 (2015)
11. B. Geng, G. Wang, Z. Jiang, T. Xie, S. Sun, G. Meng, L. Zhang, *Appl. Phys. Lett.* **82**, 4791 (2003)
12. A. Khare, S. Bhushan, *Eff. Defects Solids* **161**, 631 (2006)
13. B.N. Patil, D.B. Nai, V.S. Shrivastava, *Chalcogenide Lett.* **8**, 117 (2011)
14. S. Stolyarova, M. Weinstein, Y. Nemirovsky, *J. Cryst. Growth* **310**, 1674 (2008)
15. A.A. Albassan, *J. Solar Energy Mater. Solar Cells* **57**, 323 (1999)
16. T. Yamaguchi, Y. Yamamoto, T. Tanaka, T. Demizu, A. Yoshida, *Thin Solid Films* **281–282**, 375 (1996)
17. S. Jana, R. Maity, S. Das, M.K. Mitra, K.K. Chattopadhyay, *Phys. E* **39**, 109 (2007)
18. A. Hasnat, J. Podder, *J. Sci. Res.* **4**, 11 (2012)
19. M. Muthusamy, S. Muthukumar, M. Ashokkumar, *Ceramics Inter.* **40**, 10657 (2014)
20. M.T.S. Nair, P.K. Nair, *Semicond. Sci. Technol.* **4**, 191 (1989)
21. A.A. Ziabari, F.E. Ghodsi, *Growth. Sol. Energy Mater. Sol. Cells* **105**, 249 (2012)
22. I. Kaur, D.K. Pandya, K.L. Chopra, *J. Electrochem. Soc.* **127**, 943 (1980)
23. O. Portillo-Moreno, H. Lima-Lima, V. Ramírez-Falcon, J. Martínez-Juárez, G. Juárez-Díaz, R. Lozada-Morales, B. Rebollo-Plata, R. Palomino-Merino, O. Zelaya-Angel, *J. Electrochem. Soc.* **153**, G926 (2006)
24. J.L. Martinez-Montes, G. Martinez, G. Torres-Delgado, O. Guzmán, O. Zelaya-Angel, R. Lozada-Morales, *J. Mater. Sci. Mater. Electron.* **8**, 399 (1997)
25. H.H. Afify, I.K. El Zawawi, I.K. Battisha, *J. Mater. Sci. Mater. Elect.* **10**, 497 (1999)
26. P. Reyes, S. Velumani, *Mater. Sci. Eng. B* **177**, 1452 (2012)
27. T. Abe, J. Sato, S. Ohashi, M. Watanabe, Y. Kashiwaba, *Phys. Stat. Sol. B* **229**, 1015 (2002)
28. R.W. Meulenberg, T. van Buren, K.M. Hanif, T.M. Willey, G.F. Strouse, L.J. Terminello, *Nano Lett.* **4**, 2277 (2004)
29. J. Huheey, *Inorganic Chemistry*, 3rd edn. (Harper and Row, New York, 1983)
30. D. Anbuselvan, S. Muthukumar, *Optical Mater.* **42**, 124 (2015)
31. R. Sangeetha, S. Muthukumar, M. Ashokkumar, *Spectrochim. Acta Part A Mol. Biomol. Spectrosc.* **144**, 1 (2015)
32. R. Mariappan, V. Ponnuswamy, M. Ragavendar, D. Krishnamoorthi, C. Sankar, *Optik* **123**, 1098 (2012)
33. S. Kose, F. Atay, V. Bilgin, I. Akyuz, E. Ketenci, *Appl. Surf. Sci.* **256**, 4299 (2010)
34. H. Khallaf, I.O. Oladeji, L. Chow, *Thin Solid Films* **516**, 5967 (2008)
35. F. Liu, Y. Lai, J. Liu, B. Wang, S. Kuang, Zh. Zhang, J. Li, Y. Liu, *J. Alloys Compd.* **493**, 305 (2010)
36. A. Mondal, T.K. Chaudhuri, P. Pramanik, *Solar Energy Mater.* **7**, 431 (1982)
37. A.I. Oliva, O.S. Canto, R.C. Rodrigues, P. Quintana, *Thin Solid Films* **391**, 28 (2001)
38. M. Ashokkumar, S. Muthukumar, *Phys. E* **69**, 354 (2015)
39. F. Kadirghan, D. Mao, W. Song, T. Ohono, B. Mccandless, *Turk. J. Chem.* **24**, 21 (2000)
40. J. Akintunde, *J. Mater. Sci. Mater. Electron.* **11**, 503 (2000)
41. P.Y. Yu, M. Cardona, *Fundamentals of Semiconductors* (Springer, New York, 2001)
42. N. Chestony, T.D. Harris, R. Hull, L.E. Brus, *J. Phys. Chem.* **90**, 3393 (1986)
43. Y. Sun, N.G. Ndifor-Angwafor, D.J. Riley, M.N.R. Ashfold, *Chem. Phys. Lett.* **431**, 352 (2006)
44. C. Wang, H.M. Wang, Z.Y. Fang, *J. Alloys Compd.* **486**, 702 (2009)